

## DOUBLE SUBSTITUTED CARBONATED HYDROXYAPATITE FOR STONE CONSOLIDATION

LORENA IANCU<sup>1,2\*</sup>, RODICA-MARIANA ION<sup>1,2</sup>, RAMONA MARINA GRIGORESCU<sup>1</sup>,  
MADALINA ELENA DAVID<sup>1,2</sup>, MARIUS GHIUREA<sup>1</sup>, GABRIEL VASILIEVICI<sup>1</sup>,  
RALUCA MARIA STIRBESCU<sup>3</sup>, IOANA DANIELA DULAMA<sup>3</sup>

Manuscript received: 01.07.2020; Accepted paper: 10.08.2020;

Published online: 30.09.2020.

**Abstract.** This paper aims with the preparation of  $Sr^{2+}$  and  $Zn^{2+}$  double substituted carbonated hydroxyapatite (Sr-Zn-CHAp) by the nanoemulsion method and to evaluate its consolidation capacity on artificial stone samples. The changes in CHAp lattice parameters were observed by a synergy between the shrinkage and dilatation induced by the two metallic ions, with different ionic radii by comparison with calcium. The changed morphology obtained by calcination was evidenced by SEM analysis. Also, the tendency to agglomerate of the double substituted CHAp as micron- and sub-micron-sized particles with spherical and irregular form was observed. The FTIR, XRD and EDS results confirmed that the CHAp was successfully substituted with  $Sr^{2+}$  and  $Zn^{2+}$  by replacing  $Ca^{2+}$  resulting a AB-type CHAp. The efficacy of Sr-Zn-CHAp as inorganic consolidant for the stone was tested by mechanical strength, resistance at freeze-thaw artificial aging test, thermal shock weathering, colorimetric changes of the artificial stone sample, all the results being correlated with the water absorption test, water repellency, and pore structure changes. By treating the stone with 0.5 g/L Sr-Zn-CHAp led to an improvement of the above-mentioned characteristics, without significant chromatic changes.

**Keywords:** carbonated hydroxyapatite double substituted; nanoemulsion technique; structural characterization; morphology; stone consolidation.

### 1. INTRODUCTION

Carbonated hydroxyapatite (CHAp) is an inorganic compound with various applications, including the medical field [1-4], as well as in the conservation and preservation of cultural heritage [5-7]. Apatite is characterized by a hexagonal lattice of tetrahedral  $PO_4^{3-}$  that has interstitial sites where  $Ca^{2+}$  is located. The general formula of apatite is  $Ca_{10}(PO_4)_6X_2$  and X can be F - fluorapatite, OH - hydroxyapatite, or Cl - chlorapatite. The apatite lattice is very susceptible to substitution or vacancies and X can be easily replace with  $\frac{1}{2}CO_3$  or  $\frac{1}{2}O$ ,  $Ca^{2+}$  can be substituted by metallic ions (Sr, Ba, Zn, Na etc.), and  $PO_4^{3-}$  by  $HPO_4^{2-}$  or  $CO_3^{2-}$  [8]. CHAp can be obtained by replacing the phosphate and/or the hydroxyl groups from the apatite structure with carbonate groups, and thus A-CHAp (by replacing  $PO_4^{3-}$ ), B-CHAp (by replacing the  $OH^-$ ), or AB-CHAp can be obtained. In some application, osteoinductivity and

<sup>1</sup> National R&D Institute for Chemistry and Petrochemistry – ICECHIM, Research Group „Evaluation and Conservation of Cultural Heritage“, Bucharest, Romania.

<sup>2</sup> Valahia University of Târgoviște, Doctoral School of Materials Engineering, 130105 Targoviste, Romania.

<sup>3</sup> Valahia University of Targoviste, Institute of Multidisciplinary Research for Science and Technology, 130004 Targoviste, Romania.

\* Corresponding author: [lorenna77ro@yahoo.com](mailto:lorenna77ro@yahoo.com).

antimicrobial properties can be obtained by the insertion into the structure of metallic ions, like  $\text{Sr}^{2+}$  and  $\text{Zn}^{2+}$ , by replacing  $\text{Ca}^{2+}$  from CHAp [5, 9, 10].

Substituted hydroxyapatite (HA) can be synthesized by various procedures such as sol-gel [11], hydrothermal [12], precipitation [13, 14] and nanoemulsion techniques [15]. The synthesis of double substituted hydroxyapatites can be performed either by a solid-state route or by an aqueous precipitation method [9, 10]. Lowry and co-workers [9] have successfully synthesize nanoscale hydroxyapatite co-substituted with strontium and zinc ions in different concentrations using an aqueous precipitation method. HA containing 2 mole % Sr, 10 mol% Mg, or 2 mol% Zn have been obtained by Cox through a precipitation method [10]. The incorporation of  $\text{Sr}^{2+}$  cations into the hydroxyapatite structure improves the physico-chemical properties of apatite [16-18]. In previous research [5], the characterization of synthesized CHAp with different dopants (Ag, Sr, Ba, K, Zn), evidenced the inclusion of these metallic ions into the apatite structure by replacing the calcium ions. Similar morphology compared to CHAp was also observed.

Presently, studies have been carried out using experimental laboratory simulations to assess stone durability produced by freeze-thaw test, thermal shock weathering and salt crystallization [19, 20]. The modification in pore size distribution is an important parameter, because it determines limestone durability to ice and salt crystallization cycles [21], and an increased crystallization pressure [22]. In our previous research [5], the resistance to artificial weathering (freeze-thaw), pore structure changes, water absorption, and compressive strength of artificial stone samples were evaluated after brushing and spraying CHAp and metallic derivatives of CHAp as efficient consolidate agents of stone. Improved properties were obtained using various metallic derivatives of CHAp applied by brushing. Homogeneous and strong coatings deposited on the stone surface led to better resistance to water uptake and weathering. The efficiency of the consolidation treatment was influenced by the method of application of the consolidating agent, the solution concentration, and the amounts of the absorbed consolidate on the stone surface.

In this paper, for the first time in literature, the nanoemulsion method to form carbonated hydroxyapatite double substituted with strontium and zinc was reported. Sr-Zn-CHAp was investigated by Fourier Transform Infrared Spectroscopy, Raman Spectroscopy, X-Ray Diffraction and Scanning Electron Microscopy with Energy Dispersive Spectroscopy (SEM-EDS) techniques and porosimetry. The effectiveness of Sr-Zn-CHAp as consolidate for artificial stone was evaluated in terms of mechanical strength, water drop absorption, water repellency, and resistance at freeze-thaw and thermal shock artificial aging test, color alteration, optical microscopy, and pore structure changes.

## 2. MATERIALS AND METHODS

### 2.1. SYNTHESIS OF CARBONATED HYDROXYAPATITE DOUBLE SUBSTITUTED WITH STRONTIUM AND ZINC

Sr-Zn-CHAp was obtained by the nanoemulsion technique which involves the addition of  $\text{Sr}^{2+}$  and  $\text{Zn}^{2+}$  precursors to partially replace  $\text{Ca}^{2+}$  ions in the apatite structure. Aqueous solutions of di-ammonium hydrogen phosphate ( $(\text{NH}_4)_2\text{HPO}_4$ ) and ammonium bicarbonate ( $\text{NH}_4\text{HCO}_3$ ) were mixed under magnetic stirring. The pH of the aqueous solution was adjusted to 11 using sodium hydroxide (NaOH) 1M. Then an acetone solution of  $\text{Ca}(\text{NO}_3)_2 \cdot 4\text{H}_2\text{O}$ , 2.5 mol% strontium nitrate ( $\text{Sr}(\text{NO}_3)_2$ ) and 2.5 mol% zinc nitrate

( $\text{Zn}(\text{NO}_3)_2 \cdot 6\text{H}_2\text{O}$ ) were added simultaneously. The reaction was carried out at room temperature. The obtained white precipitate was vacuum filtered using a Buchner funnel and washed 3 times with distilled water. The reaction product was freeze-dried overnight, and then calcinated at  $900^\circ\text{C}$  for 4 h.

## 2.2. PREPARATION AND TREATMENT OF ARTIFICIAL STONE SAMPLES

The cubic stones with  $40 \times 40 \times 40$  mm dimensions were prepared from sand, lime, gypsum (1:1:2) and water, Figure 1. Sr-Zn-CHAp solutions of 0.1 g/L 0.25 g/L and 0.5 g/L were prepared by ultrasonication for 60 minutes at  $40^\circ\text{C}$  and applied by brushing for 3 times on each cube face of the artificial stone. After treatment, the stone samples were dried for 48 hours at room temperature. Based on the tests achieved on artificial stones, the most efficient concentration of the Sr-Zn-CHAp consolidate agent could be selected.



Figure 1. Artificial stones.

## 2.3. METHODS OF CHARACTERIZATION Sr-Zn-CHAp

*Fourier transformed infrared spectroscopy (FTIR)* was performed with single-bounce diamond-attenuated total reflectance (ATR) using a Vertex 80v spectrometer (Bruker Optik GMBH, Ettlingen, Germany), equipped with DRIFT accessory in the range of  $4000\text{--}400\text{ cm}^{-1}$ .

*Raman spectra* was recorded using a Raman wavelength portable analyzer (Rigaku, Woodlands, TX, United States of America) equipped with 785 and 1064 nm stabilized laser, providing high sensitivity. For measurements, a resolution of  $4\text{ cm}^{-1}$  with a laser power of 252 mW was used. The data were collected and processed with the Opus 7.0 software (Bruker Optics GmbH).

*X-ray diffraction (XRD)* spectrum was recorded with a Rigaku Ultima IV diffractometer (Rigaku, Tokyo, Japan) using a  $\text{Cu K}\alpha$  radiation ( $\lambda = 1.54\text{ \AA}$ ). In this experiment the accelerating voltage of the generator radiation was set at 40 kV and the emission current at 200 mA. The diffractogram was performed through the scanning range  $2\theta = 10^\circ - 60^\circ$ , at a scan rate of  $4^\circ/\text{min}$ .

*Scanning Electron Microscopy coupled with Energy Dispersive Spectroscopy (SEM-EDS)* data were achieved using a SU-70 microscope (Hitachi, Japan) and UltraDry detector (Thermo Fisher Scientific, USA). This system allows obtaining high-resolution images at micro- and nanoscale, as well as, qualitative and quantitative elemental analysis at the sample surface.

The *porosity* and pore size was determined, by way of the nitrogen adsorption/desorption isotherms at 77 K in the relative pressure range  $p/p_0 = 0.005-1.0$  using NOVA2200e Gas Sorption Analyzer (Quantachrome, Boynton Beach, FL, USA) with version 11.03 software. The Brunauer-Emmett-Teller (BET) equation was applied for the determination of surface area. For pore size determination was applied the Barret-Joyner-Halenda (BJH) method.

## 2.4. TESTING METHODS FOR ARTIFICIAL STONE

*Water absorption* measurement is a simple method, useful in the laboratory to characterize porous building materials, to assess the deterioration degree and to monitor the effectiveness of conservation treatments. Total water absorption represents the amount of water absorbed by the material by immersion in distilled water, at room temperature and pressure, expressed as a percentage of the dry mass of the sample. For the water absorption test the samples were dried in an oven at 40°C for 8 hours and then cooled and weighed ( $W_1$ ). After that, the specimens were immersed in distilled water at room temperature for 24 hours and weighed ( $W_2$ ). Water absorption was calculated with Equation (1) and expressed as percent.

$$\text{Water absorption (\%)} = [(W_2 - W_1)/W_1] * 100 \quad (1)$$

*Water repellency* (WR) represents the resistance of the stone surface to the absorption of water, and was carried out using a procedure adapted from [23] and calculated based on Equation (2). The water drop absorption (WA) represents the absorption time of a limited and defined amount of water on the surface of a material, and was expressed following on Equation (3). For the water drop absorption test, the samples were dried in the oven at 60°C for 24 h and cooled at room temperature. After that, distilled water (1 mL) was dropped onto the sample surface from 1 cm height using a burette. The time for the total absorption of the water was measured as  $t_x$  (absorption time into a treated or weathered surface, min) and  $t_n$  (absorption into the control untreated surface, min).

$$WR (\%) = 100 - WA \quad (2)$$

$$WA (\%) = \left[ 1 - \frac{t_x - t_n}{t_x} \right] \cdot 100 \quad (3)$$

*Mechanical strength* was determined using a Silver Schmidt Proceq test hammer, type L, with 0.735 Nm impact energy, according to ASTM C805. Ten measurements at a minimum spacing of 25 mm between each two testing points and a minimum edge distance of 25 mm have been recorded for control and each artificial stone sample. The compressive strength was calculated using the Equation (4) (for 10<sup>th</sup> percentile curve range), according to equipment manual:

$$\text{Compressive strength} = 2.77 * e^{0.048*Q} \quad (4)$$

where Q – rebound number and 2.77 – constant of the apparatus.

*Freeze-thaw artificial test* (FT) is used to check the resistance of the material to frost and was performed according to STAS 6200/15 83. The samples were first dried in an oven at

105±5°C for 1 hour. A freeze-thaw cycle consisted in samples immersion in distilled water for 15 minutes at room temperature, freezing them for 3 hours at a temperature of -18±5°C and thawing in distilled water for 1 hour. 20 cycles of freeze–thaw operation was performed and the mass losses expressed as gelivity coefficient was calculated using Equation (5).

$$\% \mu_g = \left( m_2 - \frac{m_3}{m_1} \right) * 100 \quad (5)$$

where:  $m_1$ –the initial mass of the sample, after drying at 105 °C, in grams;  $m_2$ –mass of sample saturated with water, determined before the first freeze–thaw cycle, in grams;  $m_3$ – the final mass of weathered sample, after the last cycle, in grams.

*Thermal shock weathering (TS)* test was carried out on cubic samples (40x40x40 mm) of control and Sr-Zn-CHAp treated artificial stones, according to SIST EN 14066/2013 [24]. The stones were dried until constant mass, weighed and then weathered by heating in an oven at 70°C for 18 h and immersion in distilled water at 20°C for 6 h. Each cycle of the thermal shock was repeated 10 times. At the end of the cycles, the specimens were dried in an oven, weighed, and the loosed percent of mass was calculated, according to Equation (6):

$$\% \Delta m = (m_f - m_0/m_0) * 100 \quad (6)$$

where:  $m_0$  - the initial mass of the sample, determined after drying at 70°C to the constant mass, in grams;  $m_f$  - the final mass of the sample, in grams.

*Chromatic parameters* of the treated stones have been recorded with a CR-410 colorimeter (Konica Minolta, Tokyo, Japan). Determinations were made for both the control and the samples treated with carbonated hydroxyapatite co-substituted with strontium and zinc. The measurements were expressed following the CIE L\* a\* b\* systems. The total color differences  $\Delta E_{x\text{final}}$  was estimated according to EN 15886 [25] and ASTM 2244 [26], and calculated using Equation (7):

$$\Delta E_{x\text{final}} = (\Delta L_x^2 + \Delta a_x^2 + \Delta b_x^2)^{1/2} \quad (7)$$

where,  $\Delta L$  is the difference in lightness ( $\Delta L = L_{\text{treated stone}} - L_{\text{control}}$ ),  $\Delta a$  is the chromatic deviation of the a coordinates (red and green color) ( $\Delta a = a_{\text{treated stone}} - a_{\text{control}}$ ), and  $\Delta b$  is chromatic deviation of the b coordinates (yellow and blue color) ( $\Delta b = b_{\text{treated stone}} - b_{\text{control}}$ ).

*Optical microscopy (OM)* was recorded with a Novex trinocular microscop that offers the possibility of investigating the samples in transmitted light at a magnification between 4–100X. The equipment had a digital video camera attached (Axiocam 105, Carl Zeiss, Oberkochen, Germany) which, by the microscope software, allowed real-time data acquisition.

### 3. RESULTS AND DISCUSSION

Fourier transform infrared spectroscopy (FTIR) is a chemical analysis technique that determines the molecular structure of the samples. FTIR spectra of carbonated hydroxyapatite double substituted with strontium and zinc dried (non-calcinated) and calcinated at 900°C is presented at Fig. 2. By thermal treatment, the band corresponding to the –OH group from 3300-3500  $\text{cm}^{-1}$  disappears; the broad absorption indicates the adsorbed water into the hydroxyapatite structure. The band characteristic to water deformation in case of non-calcinated Sr-Zn-CHAp appear also at 1635  $\text{cm}^{-1}$  [27]. Also, the 400-600  $\text{cm}^{-1}$  band (bending

vibration band) assigned to the phosphate group can indicate an improved crystallinity obtained by calcination.

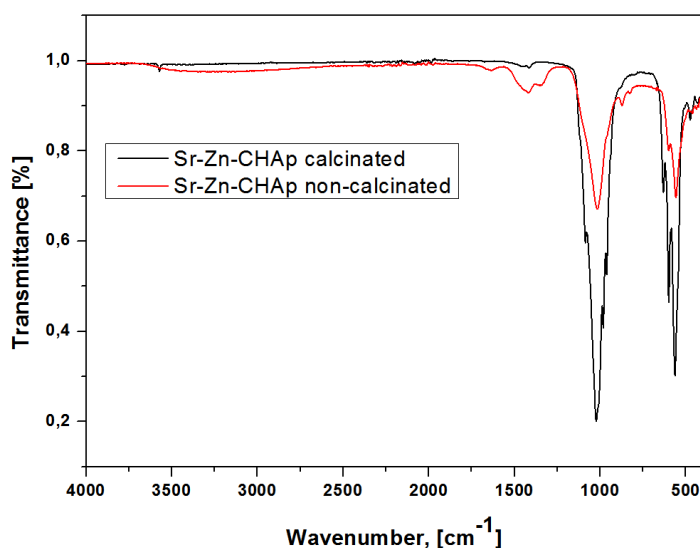


**Figure 2.** FTIR spectra of carbonated hydroxyapatite co-substituted with strontium and zinc, non-calcinated and calcinated.

For non-calcinated Sr-Zn-CHAp, the two small peaks between 1350 and 1440  $\text{cm}^{-1}$  and the band from 875  $\text{cm}^{-1}$  can be assigned to the  $\nu_3$  stretching, respectively to  $\nu_2$  bending modes of carbonate ions that can substitute the phosphate site in a B-type apatite. The  $\nu_3$  asymmetric stretching of P-O bond of  $\text{PO}_4^{3-}$  group appear at 1020  $\text{cm}^{-1}$  [28]. The bands from 560-610  $\text{cm}^{-1}$  can be assigned for the  $\nu_4$  O-P-O bending mode [29]. In case of the calcinated sample, the two peaks for the  $\nu_3$  stretching of carbonate are merged into a single band that appear at 1438  $\text{cm}^{-1}$  and the band from 875  $\text{cm}^{-1}$  disappears, so called B-type apatite. After calcination, the bands recorded for Sr-Zn-CHAp are sharper and stronger, indicating an improvement of the crystallinity and an increase of nanoparticle sizes. Their positions indicate that  $\text{CO}_3^{2-}$  ion substitutions took place both at the OH- (A-site) and  $\text{PO}_4^{3-}$  (B-site) positions [9].

Raman spectroscopy as a non-destructive technique revealed the carbonate and phosphate vibrational modes of carbonated hydroxyapatite double substituted with strontium and zinc sample, by comparison with those of carbonated hydroxyapatite (Fig. 3).

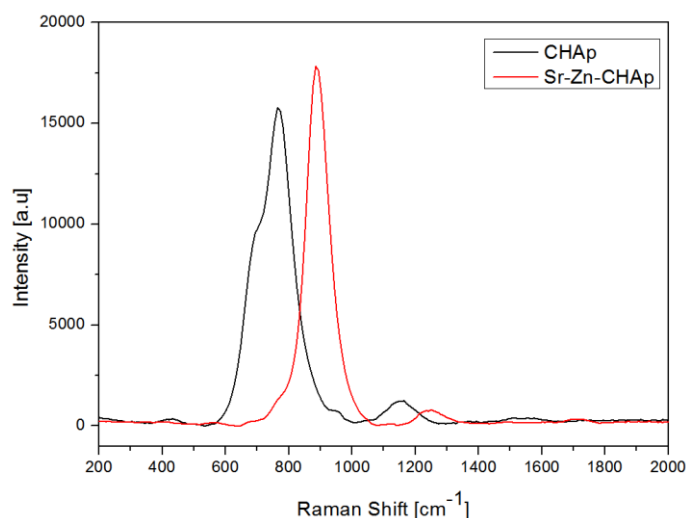


**Figure 3.** Raman spectrum for CHAp and CHAp-Sr-Zn samples.

According to literature, the characteristic bands for  $\text{PO}_4^{3-}$  groups in the Raman spectrum of synthetic hydroxyapatite are:  $1075\text{ cm}^{-1}$  ( $\nu_3$ ),  $1029\text{--}1048\text{ cm}^{-1}$  ( $\nu_3$ ),  $948\text{--}962\text{ cm}^{-1}$  ( $\nu_1$ ),  $584\text{--}602\text{ cm}^{-1}$  ( $\nu_4$ ),  $430\text{--}450\text{ cm}^{-1}$  ( $\nu_2$ ). The band at  $1070\text{ cm}^{-1}$  can be assigned to  $\text{CO}_3^{2-}$  stretching vibration modes ( $\nu_1$ ) in a B-type carbonate apatite. The characteristic band of hydroxyapatite is at approximate  $960\text{ cm}^{-1}$  for symmetric stretching vibrations of O–P–O bonds [30]. In B-CHAp of the  $\nu_1$  mode of phosphate at  $964\text{ cm}^{-1}$  for hydroxyapatite presented a slight wavenumber modification and observed a single band at approximate  $960\text{ cm}^{-1}$ . In case of A-CHAp, on the contrary exhibited two bands, the most intense at  $957\text{ cm}^{-1}$ , and at  $947\text{ cm}^{-1}$  [31].

X-ray diffraction was used for determining the phase purity, degree of crystallinity, crystal size and lattice parameters of carbonated hydroxyapatite double substituted with strontium and zinc. The registered XRD spectrum of the synthesized and calcinated Sr-Zn-CHAp at  $900^\circ\text{ C}$  temperature is presented in Fig. 4. Analyzing the spectrum, it can be observed the specific peaks for hydroxyapatite (ICDD 01-076-0694). The  $2\theta$  values and their intensities suggest the lack of impurities into the sample.

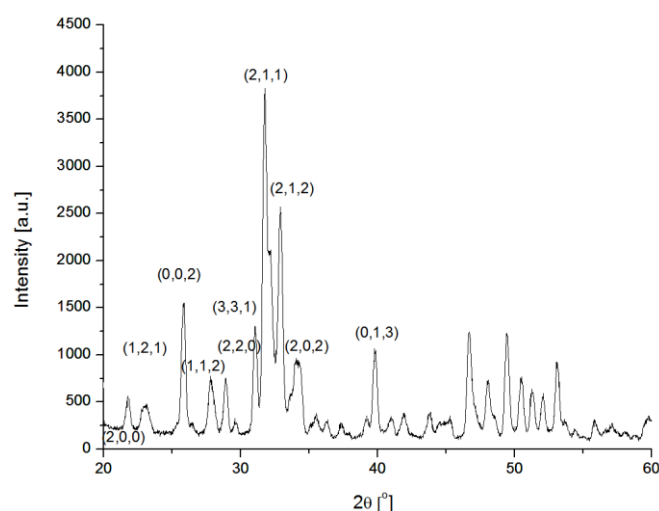


Figure 4. XRD diffractogram for Sr-Zn-CHAp.

The influence of calcium substitution with the two metallic cations on the lattice parameters was also studied by analysis the  $2\theta$  value, the inter-planar distance ( $d$ ), the full-width at half-maximum of the peak ( $\beta$ ) and the crystallite size ( $L$ ) of the Sr-Zn-CHAp sample estimated using the Scherrer's Equation (8) (with a  $K$  constant of 0.9 and the measurement X-ray wavelength  $\lambda$  of  $1.54\text{ \AA}$ ). These values are presented in Table 1.

$$L = \frac{K \cdot \lambda}{\beta \cdot \cos\theta} \quad (8)$$

Table 1. The crystallite dimension of Sr-Zn-CHAp in comparison with the CHAp.

CHAp [5]				Sr-Zn-CHAp				Miller index
$2\theta$ [°]	$d$ [Å]	$\beta$ [Å]	$L$ [Å]	$2\theta$ [°]	$d$ [Å]	$\beta$ [Å]	$L$ [Å]	
10.81	8.179	0.366	242.28	10.82	8.171	0.3725	238.05	(1, 0, 0)
16.93	5.233	0.3329	268.10	16.92	5.236	0.4092	218.11	(1, 0, 1)
21.77	4.080	0.3501	256.77	21.75	4.083	0.3637	247.16	(2, 0, 0)
25.80	3.451	0.3460	261.74	25.80	3.451	0.3395	266.76	(0, 0, 2)
27.76	3.211	0.3577	254.22	27.80	3.207	0.4925	184.65	(1, 0, 2)
28.90	3.087	0.3536	257.81	28.86	3.091	0.3255	280.04	(2, 1, 0)
31.74	2.817	0.3217	285.28	31.73	2.818	0.2741	334.81	(2, 1, 1)
32.30	2.770	0.7073	129.94	31.11	2.873	0.6148	149.05	(1, 1, 2)
32.93	2.718	0.3356	274.29	32.91	2.720	0.4001	230.06	(3, 0, 0)

As can be seen from Table 1, the specific peaks for Sr-Zn-CHAp appear at slightly modified angles compared to CHAp, to the left, but also to the right. The shift to the left can be explained using the ionic radius ( $r_{\text{ion}}$ ) that is larger for  $\text{Sr}^{2+}$  (1.12 Å) that have substituted the  $\text{Ca}^{2+}$  ions with a smaller ionic radius (0.99 Å) [32]. Some of the peaks are shifted to right as the  $\text{Zn}^{2+}$ , having a smaller ionic radius 0.74 Å, by substituting calcium into the hydroxyapatite structure cause a shrinkage in the unit cell parameters. But using the two metallic ions, with ionic radii different from that of the substituted ion, leads to a synergy between the shrinkage and dilatation of the unit cell.

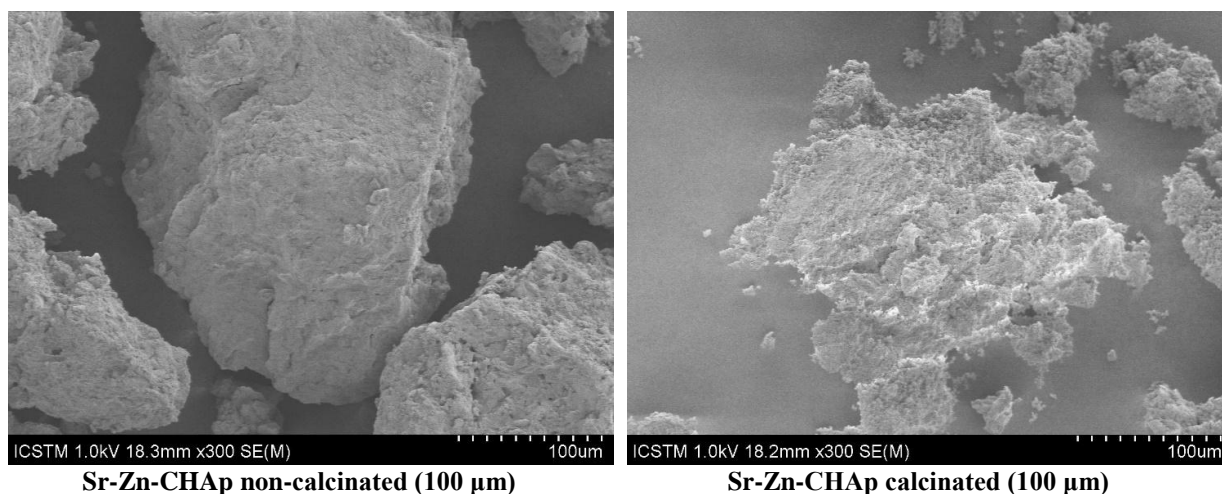
The XRD pattern of Sr-Zn-CHAp shows sharper peaks by comparison with CHAp, which can be associated with an increased crystallinity induced by the two metallic ions. This had to be correlated with a decrease of the crystallite size [10]. For the obtained double substituted CHAp, a higher polydispersity of the values was observed. The L values are smaller (with up 70 Å) compared to the simple CHAp, this being a proof of achieving the calcium ions substitution with strontium and zinc.

Different studies have been carried out in order to study the influence of carbonate substitution on lattice parameters of hydroxyapatite. It has been reported that the modifications appears according to types of  $\text{CO}_3$  substitution (A, B and AB) [31]. By replacing  $\text{Ca}^{2+}$  with larger ions (in our case  $\text{Sr}^{2+}$ ), the main change in lattice parameters is observed for a and c values [8]. The value of the ionic radius is invers proportional with the lattice constants. The a and c parameters were calculated using the Equation (9), specific for hexagonal crystal structures, based in the inter-planar distance and Miller indexes. A was calculated for the (3, 0, 0) and (2, 1, 0) peaks, and c was calculated for the (0, 0, 2) and (2, 1, 1).

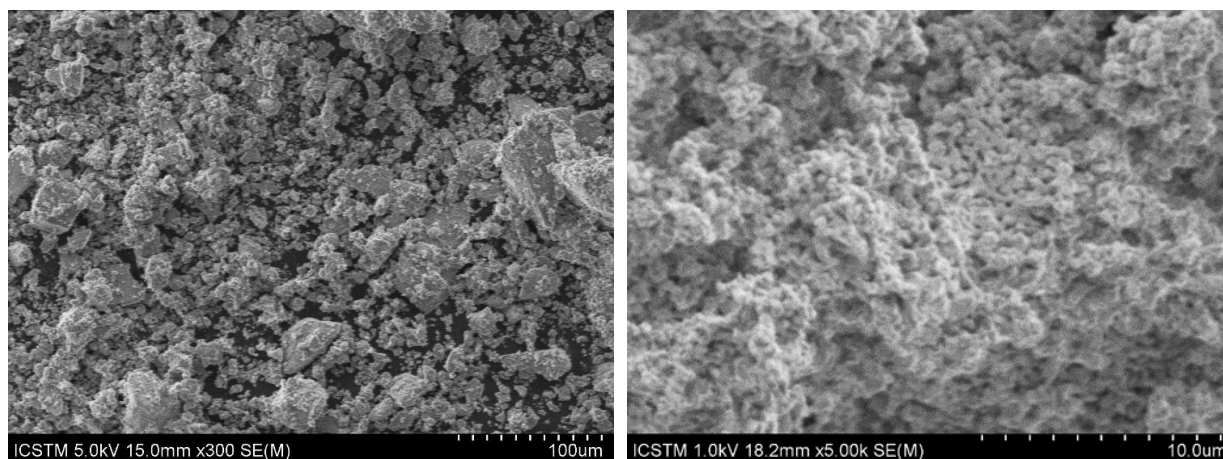
$$\frac{1}{d^2} = \frac{4}{3} \cdot \frac{h^2 + hk + k^2}{a^2} + \frac{l^2}{c^2} \quad (9)$$

Compared to CHAp (a=9.431 and c=6.891) [5], for Sr-Zn-CHAp increased values were obtained, respectively 9.4328 for a, and 6.902 for c. The values for the both CHAp correspond to the apatite structure and their increase proved the lattice substitutions. The expansion along the a and c axes and the CHAp lattice substitution led to an increase of the unit cell from 529.6 Å<sup>3</sup> for CHAp to 531.6 Å<sup>3</sup>.

The morphology of Sr-Zn-CHAp dried and calcinated, in comparison with CHAp, achieved by SEM is presented in Fig. 5.







**CHAp (100  $\mu\text{m}$ )** **Sr-Zn-CHAp non-calcinated (10  $\mu\text{m}$ )**  
**Figure 5. SEM images for Sr-Zn-CHAp calcinated and non-calcinated in comparison with CHAp.**

By SEM analysis, a change in morphology by calcination could be observed. The compact form of Sr-Zn-CHAp just dried becomes a porous one, with smaller particle's dimensions. The literature presents the assembly phenomenon of particles of calcium phosphate, including carbonated hydroxyapatite [33, 34]. The SEM micrographs show that, both CHAp and double-substituted CHAp exist as spherulites agglomerates in micrometric scale. By calcination, due to the high temperature, the particles agglomeration is less pronounced compared to the dried Sr-Zn-CHAp and single particles with spherical and irregular form and 700-800 nm size can be observed. Analyzing at a smaller scale, the formation of micron- and sub-micron-sized particles as well as larger agglomerates can be observed. The tendency to agglomerated of strontium doped CHAp was also observed previous in our paper [5].

In Fig. 6 are showed the compositions determined by EDS analysis for the carbonated hydroxyapatite and carbonated hydroxyapatite double substituted with strontium and zinc samples.

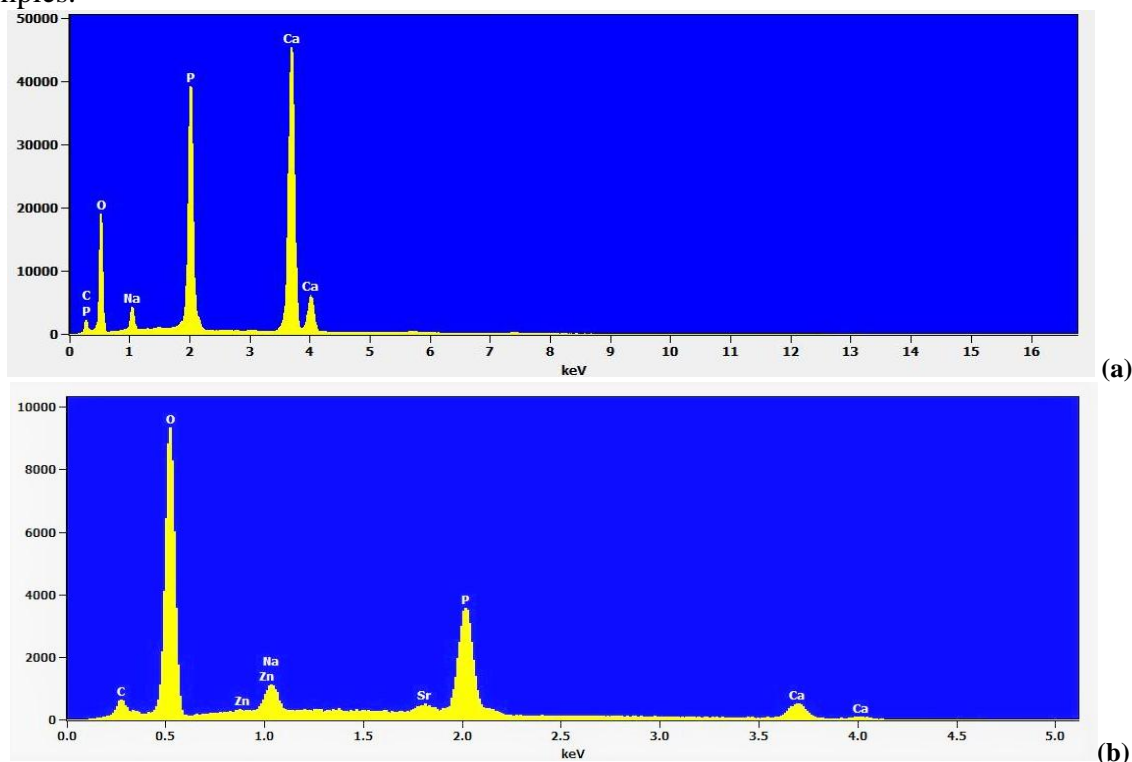


**Figure 6. EDS images for (a) CHAp and (b) Sr-Zn-CHAp.**

**Table 2. Concentration of Zn and Sr determined by EDS.**

Element /line	Element [wt. %]
Zn / L	3.67 ± 0.21
Sr / L	5.16 ± 0.36

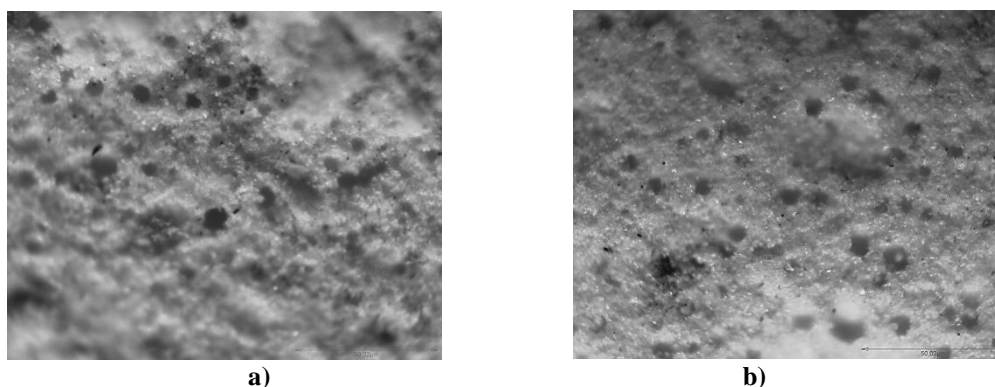
The EDS analysis confirmed the presence of Sr and Zn in substituted carbonated hydroxyapatite, by the average values (Table 2). The ability to substitute calcium is dependent on the ionic radius, as follows: higher for Sr than Zn. A very small quantity of Ca registered in the EDS spectrum is a proof for the substitution.

The durability of the stone depends of the following parameters: pore structure, namely open porosity, water absorption, specific surface area [35], and stones with narrow pores produce a low water absorption coefficient value [36, 37]. The pore structure influences their behavior under weathering condition, evaluating the degree of decay and establishing the effectiveness of conservation treatments [38]. The porosity and pore size distribution have an important role in the durability of materials [39, 40], and are key factors in controlling the water absorption within a stone [41]. The specific surface area is an important parameter for the durability of porous materials: higher surface area, less intense weathering processes [35]. The water absorption in relation to the dry weight of the stone is mainly influenced by porosity, and pore size distribution [42], also, porosity influences the mechanical properties [39, 43].

**Table 3. Surface area, pore diameter and pore volume for Sr-Zn-CHAp in comparison with CHAp samples.**

Sample	Surface area [m <sup>2</sup> /g]	Pore diameter [nm]	Pore volume [cc/g]
Sr-Zn-CHAp	2.723	2.946	0.005
Artificial stone control [5]	4.850	4.274	0.009
Sr-Zn-CHAp treated stone	62.260	4.083	0.129

The double substituted carbonated hydroxyapatite with strontium and zinc presented small values of pore diameter (2.946 nm), surface area (2.723 m<sup>2</sup>/g) and pore volume (0.005 cc/g), compared with CHAp [5], (table 4). The pores can be observed also by optical microscopy (Fig. 7).

**Figure 7. Optical microscopy of control (a) and Sr-Zn-CHAp treated (b) artificial stone (10X).**

A possible explanation for the new pores generated can be sustained by the fact that after stone treatment with Sr-Zn-CHAp, an effervescent reaction occurs with the formation and release of  $\text{CaCO}_3$  and  $\text{H}_2\text{CO}_3$ . However, this new consolidant is an efficient one, the next tests proofing its efficacy.

In order to evaluate the protective role of consolidate for porous materials, the water absorption of stone samples by total immersion can be correlated with the degree of deterioration, and monitor the effects of conservation treatment with Sr-Zn-CHAp.

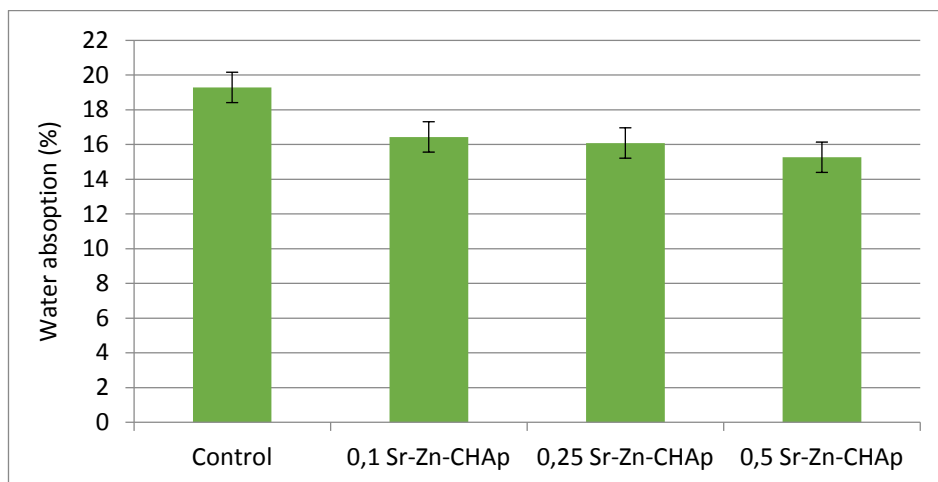


Figure 8. Water absorption for control and samples treated with Sr-Zn-CHAp.

All samples treated with Sr-Zn-CHAp (Fig. 8) showed lower water absorption than the control sample, and it was observed that water absorption decreases with increasing the concentration of consolidating agent.

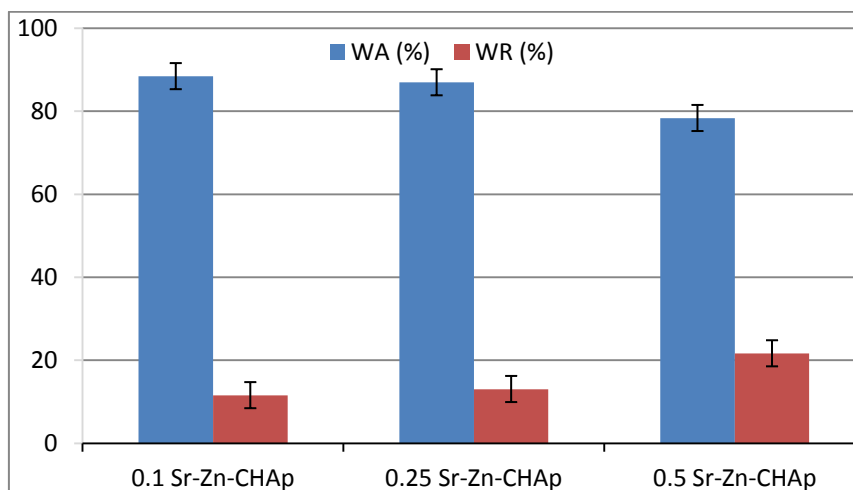
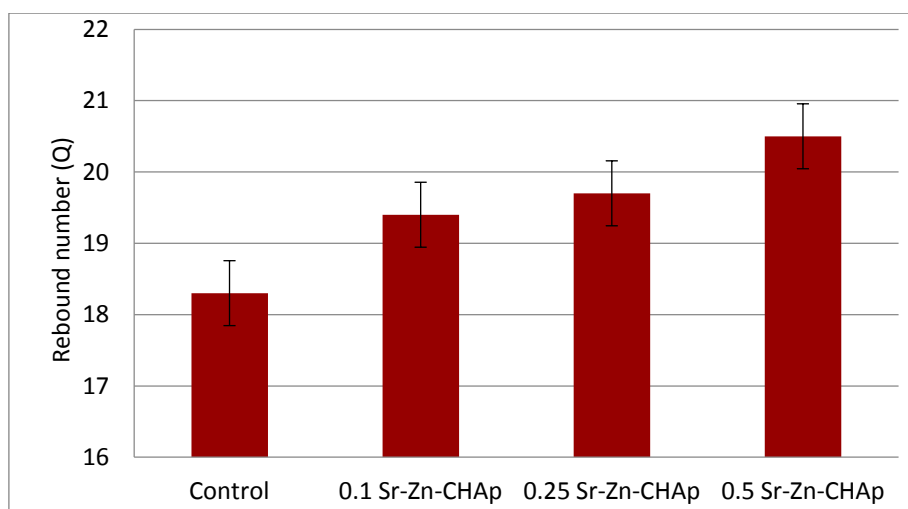


Figure 9. Water repellency and water drop absorption for stone treated with Sr-Zn-CHAp.

From Fig. 9, could be concluded that the best results were obtained for artificial stone treated with Sr-Zn-CHAp at 0.5 g/L concentration.

From mechanical point of view, carbonated hydroxyapatite co-substituted with strontium and zinc used in this study showed improved compression strength, Fig. 10. The artificial stone treated with Sr-Zn-CHAp applied by brushing at 0.5 g/L concentration shows the highest values in compressive strength. These results indicated that the addition of this consolidate had a positive effect in increasing the mechanical properties of artificial stone, with good adhesion properties.



**Figure 10. Mechanical strength for control and for stones treated with Sr-Zn-CHAp.**

The results obtained for the ratio between the compressive strength and the rebound number for the control and the samples treated with solutions of different concentrations of Sr-Zn-CHAp are shown in Figs. 11a and 11b.

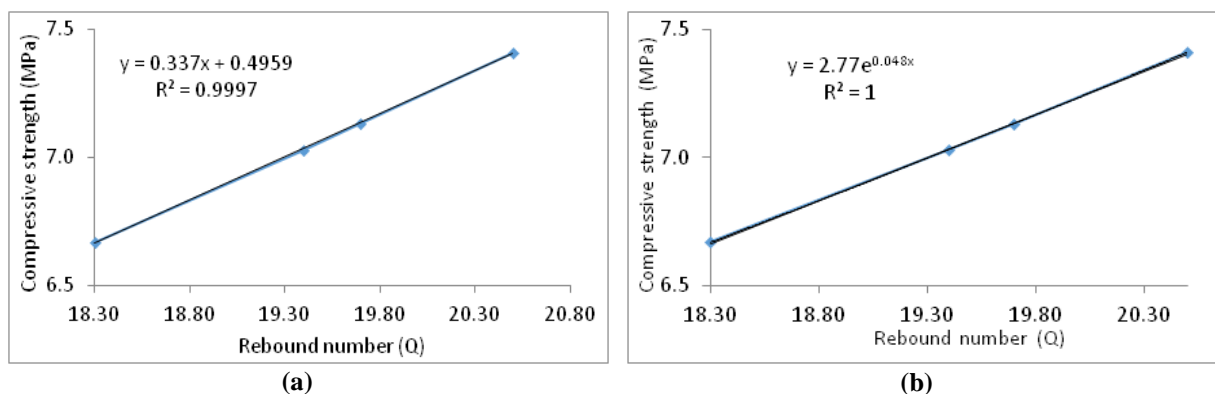














**Figure 11. The compressive strength versus rebound index relationship for artificial stones coated with Sr-Zn-CHAp. (a) - linear; (b) - exponential graphical representation.**

The linear and exponential relationship between the rebound index and the compressive strength was determined using the least squares method. As can be seen from Figs. 11a - 11b, the exponential model proved to be the best with a regression coefficient of 1, while the linear model has a regression coefficient of 0.9997, which indicates the acceptability of the exponential model for to estimate the compressive strength of artificial stones.

The low porosity to reduced water absorption capacity (Fig. 8), which results in higher values of mechanical properties, as can be seen in Fig. 10. This demonstrates a bigger better durability of the stones treated with Sr-Zn-CHAp and a decrease in vulnerability to the action of freeze-thaw cycles. The disintegration of stones subjected to the freeze-thaw test is an important process of physical degradation of buildings. The freeze-thaw test is the standard method for evaluating the durability of a rock against the stresses caused by the crystallization of ice in the pores [44].

In order to determine the alterations of the samples treated with Sr-Zn-CHAp solutions, freeze-thaw ageing test was performed. In Table 5 was presented freeze-thaw test for artificial stone treated with Sr-Zn-CHAp and in Fig. 12 gelivity coefficient. The durability of the samples was investigated after freeze-thaw and thermal shock tests by the loss weight, visual aspect of the samples and the change of the chromatic parameters.

**Table 5. Freeze–thaw test for artificial stone treated with Sr-Zn-CHAp applied by brushing.**

Sample	Initial	After 10 cycles	Final- After 20 cycles
Control			
0.1 Sr-Zn-CHAp			
0.25 Sr-Zn-CHAp			
0.5 Sr-Zn-CHAp			

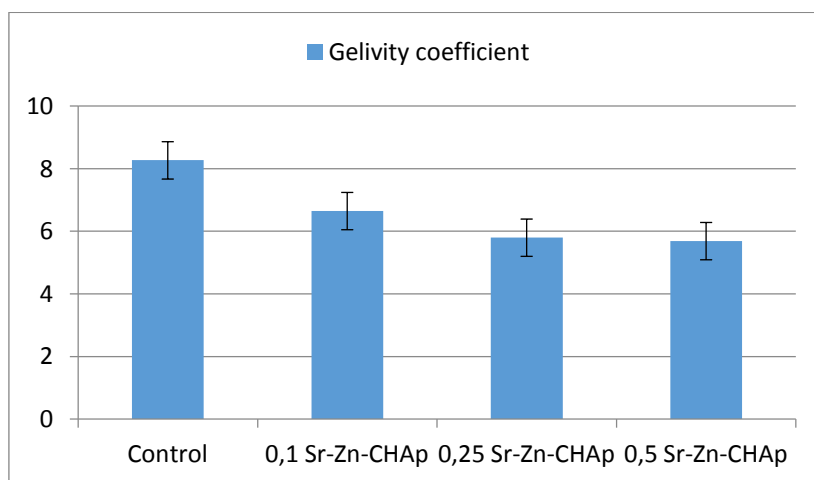














**Figure 12. Gelivity coefficient for control and for stones treated with Sr-Zn-CHAp.**



As expected, the untreated sample had the highest weight loss, while the treated stone with Sr-Zn-CHAp showed the lowest weight loss as can be observed from Fig. 12. The artificial stone treated with Sr-Zn-CHAp at 0.5 g/L concentration presented the lowest value of the gelivity coefficient and of the degradation rate, which demonstrates a greater protection capacity.

**Table 6. Samples behaviour at thermal shock test.**

Samples	Initial	After 3 cycle	After 10 cycle	Weight loss, %
Control				-0.90
0.1Sr-Zn-CHAp				-0.83
0.25Sr-Zn-CHAp				-0.71
0.5Sr-Zn-CHAp				-0.80

Colorimetric testing is a non-destructive investigation technique that provides important information about the variation of chromatic parameters before and after the application of consolidation treatment. Color measurements were performed to assess the aesthetic compatibility of the consolidating substances with the tested substrates.

The chromatic parameters for control and treated artificial stones with solutions of different concentrations of Sr-Zn-CHAp presented an insignificant color change of the  $\Delta a_x$  and  $\Delta b_x$  parameters. All stones treated with the carbonated hydroxyapatite co-substituted with strontium and zinc at different concentrations, by brushing, do not influence the color of the samples, because the total color difference compared to the control ( $\Delta E_{x\text{final}}$ ), calculated with equation (8), showed small values in the range of 3 - 5, which is in accordance with the compatibility indicators available in the literature [45-47]. The chromatic deviation of the  $\Delta a_x$

coordinate denotes that it had very small values, which do not affect the initial color of the samples after application of the consolidating agent.

The values of  $\Delta E_x$  initial decreases with increasing concentration of consolidate. The colorimetric tests of the artificial stones treated with Sr-Zn-CHAp before and after their exposure to thermal shock weathering (Fig. 13), and can be observed as both  $\Delta b_x$ , and  $\Delta E_x$  increase, after artificial aging test.

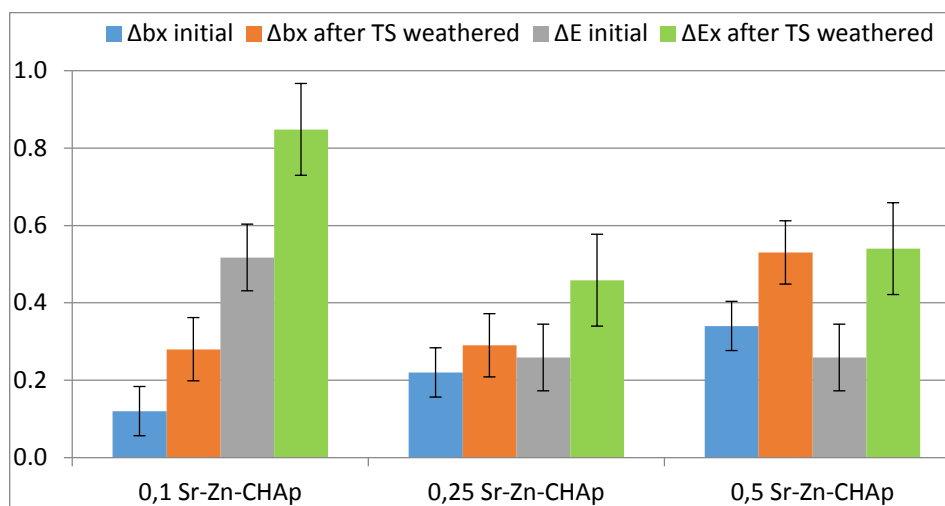


Figure 13. Chromatic parameters of the artificial stone treated with Sr-Zn-CHAp before and after their exposure to thermal shock weathering.

The effects of the freeze-thaw cycling were evaluated by measuring color difference before and after artificial aging test. The colorimetric tests of the samples before and after exposure to freeze thaw cycles, and changes of the chromatic parameters  $\Delta b_x$  and  $\Delta E_x$ , are given in Fig. 14. As can be observed after freeze thaw test  $\Delta E_x$  increase towards initial value, and  $\Delta b_x$  parameters raise in case of sample treated with Sr-Zn-CHAp at 0.1 and 0.25 concentration, but at 0.5 g/l as can be observed slowly decreases.

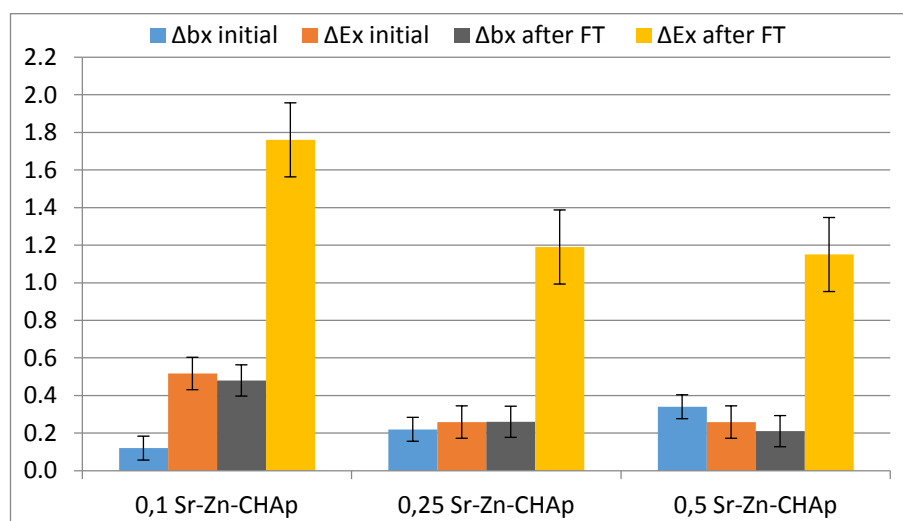
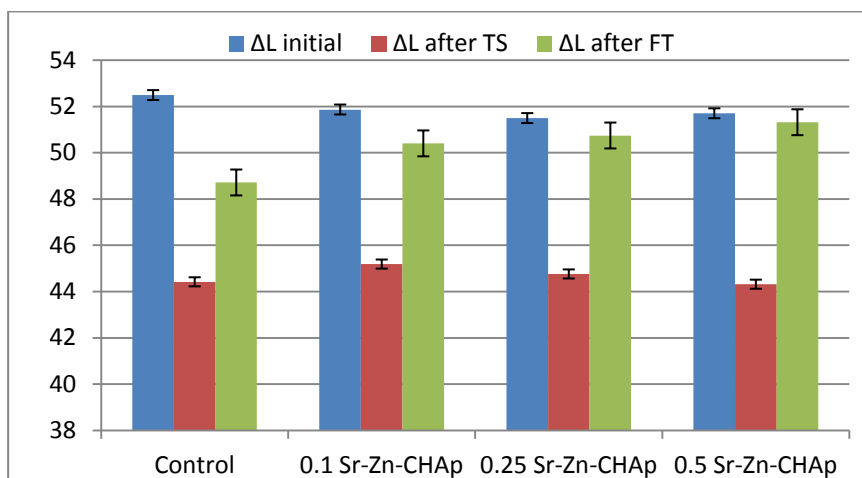


Figure 14. Chromatic parameters of the artificial stone treated with Sr-Zn-CHAp before and after their exposure to freeze-thaw artificial aging test.

The values of  $\Delta a_x$  parameter after TS increase and after FT decrease, while the lightness after artificial tests TS and FT decreases. By determining the total color difference ( $\Delta E^*$ ) between treated and untreated samples, which have been subjected to artificial aging

tests, indicated that the color properties are in direct relation to aging, because the samples after TS test shows decrease lightness and a slight reduce after FT (Fig. 15).



**Figure 15.** Lightness of the artificial stone treated with Sr-Zn-CHAp before and after their exposure to freeze–thaw and thermal shock weathering tests.

In conclusion, after the accelerated weathering tests, the freeze-thaw test is more aggressive than the thermal weathering test, because the mass loss is higher, and  $\Delta b_x$  and  $\Delta E_x$  parameters values show large variations.

#### 4. CONCLUSIONS

Carbonated hydroxyapatite double substituted with strontium and zinc (Sr-Zn-CHAp) has successfully obtained by the nanoemulsion technique, calcium ions being substituted within the crystal structure of CHAp. The results obtained by XRD and FTIR analysis demonstrated that double substituted carbonated hydroxyapatite with strontium and zinc presents a hexagonal structure with lattice parameters characteristic to synthetic hydroxyapatite. The positions of the phosphate, hydroxyl and carbonate groups indicate that  $\text{CO}_3^{2-}$  ion substitutions took place both at the OH- (A-site) and  $\text{PO}_4^{3-}$  (B-site) positions. Changes in CHAp lattice parameters were observed, but the synergy between the effects of the two ions, with different ionic radii that calcium could not be cleared. The levels of Sr and Zn substitution were measured by EDS and all expected elemental peaks were identified including Sr and Zn suggesting that substitution elements were incorporated into the carbonated hydroxyapatite.

In this study, the effectiveness of Sr-Zn-CHAp as inorganic stone consolidate has been tested by mechanical strength, resistance at freeze–thaw artificial aging test, thermal shock weathering, colorimetric tests and these results were correlated with water absorption test, water repellency, and pore structure changes. The treatment with Sr-Zn-CHAp does not influence the chromatic parameters of the artificial stones. The samples applied by brushing at 0.5 g/L concentration show the highest values in compressive strength. Sr-Zn-CHAp sample showed small values of pore diameter and higher surface area compared to CHAp. The low porosity of the sample leads to reduced water absorption capacity and results higher mechanical properties.



**Acknowledgements:** This work was supported by a grant of the Romanian Ministry of Research and Innovation, PCCDI – UEFISCDI, project number PN-III-P1-1.2-PCCDI-2017-0476 / 51PCCDI/2018, within PNCDI III.

## REFERENCES

- [1] Barralet, J., Knowles J.C., Best S., et al., *Journal of Materials Science: Materials in Medicine*, **13**(6), 529, 2002.
- [2] Syazwan, M.N.M., Marliana B.I.Y., *Materials Today: Proceedings*, **17**, 959, 2019.
- [3] Ozbek, Y., Bastan F., Ustel F., *Journal of Thermal Analysis and Calorimetry*, 125, 2016.
- [4] Kovaleva, E., Shabanov M., Putlyaev V., et al., *Central European Journal of Chemistry*, **7**, 168, 2009.
- [5] Ion, R.-M., Iancu L., Vasilievici G., et al., *Coatings*, **9**(4), 231, 2019.
- [6] Iancu, L., Ion R.-M., Grigorescu R.M., et al., *Proceedings*, **29**(1), 37, 2019.
- [7] Ion, R.-M., Nyokong T., Nwahara N., et al., *Heritage Science*, **6**(1), 37, 2018.
- [8] Elliott, J., Wilson R., Dowker S., *Advances in X-ray Analysis*, 45, 172, 2002.
- [9] Lowry, N., Brolly M., Han Y., et al., *Ceramics International*, **44**(7), 7761, 2018.
- [10] Cox, S.C., Jamshidi P., Grover L.M., et al., *Materials Science and Engineering: C*, **35**, 106, 2014.
- [11] Balamurugan, A., Balossier G., Torres P., et al., *Materials Science and Engineering: C*, **29**(3), 1006, 2009.
- [12] Lin, K., Liu P., Wei L., et al., *Chemical engineering journal*, **222**, 49, 2013.
- [13] Shen, Y., Liu J., Lin K., et al., *Materials Letters*, **70**, 76, 2012.
- [14] Zahra, N., Fayyaz M., Iqbal W., et al., *IOP Conference Series: Materials Science and Engineering. IOP Publishing*, **60**, 012056, 2014.
- [15] Zhou, W., Wang M., Cheung W., et al., *Journal of Materials Science: Materials in Medicine*, **19**(1),103, 2008.
- [16] Christoffersen, J., Christoffersen M.R., Kolthoff N., et al., *Bone*, **20**(1), 47, 1997.
- [17] Ahmed, S., Ahsan M., *Bangladesh Journal of Scientific and Industrial Research*, **43**(4), 501, 2008.
- [18] Terra, J., Dourado E.R., Eon J.-G., et al., *Physical Chemistry Chemical Physics*, **11**(3), 568, 2009.
- [19] Scherer, G.W. in *Proceedings of the 9<sup>th</sup> International Congress on Deterioration and Conservation of Stone*, Elsevier, 187, 2000.
- [20] Çelik, M.Y., Sert M., *Bulletin of Engineering Geology and the Environment*, 1, 2020.
- [21] Sassoni, E., *Materials*, **11**(4), 557, 2018.
- [22] Scherer, G.W., *Cement and Concrete research*, **29**(8), 1347, 1999.
- [23] Teutonico, J.M., *A laboratory manual for architectural conservators*, ICCROM Rome, **168**, 1988.
- [24] EN U., 14066, Natural stone test methods - Determination of resistance to ageing by thermal shock, 2013.
- [25] EN U., 15886, Conservation of cultural property. Test methods. Colour measurements of surfaces, 2010.
- [26] ASTM D. 2244, *American Society for Testing and Materials*, West Conshohocken, PA, 2003.
- [27] Zahra, G., Nounah A., Belhorma B., et al., *Journal of Materials and Environmental Science*, **6**, 983, 2015.

- [28] Zyman, Z., Tkachenko M., *Processing and Application of Ceramics*, **7**, 153, 2013.
- [29] Smith, S., Maneeprakorn W., Winotai P., *Thermochimica Acta*, **447**, 115, 2006.
- [30] Silva, C., Sombra A.B., *The Journal of physics and chemistry of solids*, **65**(5), 1031, 2004.
- [31] Krajewski, A., Mazzocchi M., Buldini P.L., et al., *Journal of Molecular Structure*, **744**, 221, 2005.
- [32] Charanworapan, C., Suddhiprakarn A., Kheoruenromne I., et al., *Soil Science and Plant Nutrition*, **59**(4),522, 2013.
- [33] Landi, E., Celotti G., Logroscino G., et al., *Journal of the European Ceramic Society*, **23**(15),2931, 2003.
- [34] Krishnan, V., Bhatia A., Varma H., *Dental Materials*, **32**(5), 646, 2016.
- [35] Benavente, D., Del Cura M.G., Fort R., et al., *Engineering geology*, **74**(1-2), 113, 2004.
- [36] Benavente, D., Lock P., Del Cura M.Á.G., et al., *Transport in porous media*, **49**(1), 59, 2002.
- [37] Ion, R.-M., Iancu L., Grigorescu R., et al., *Journal of Science and Arts*, **18**(2), 471, 2018.
- [38] Borelli, E., Urland A., *Laboratory Handbook: Conservation of Architectural Heritage. Historic Structures and Materials*, ICCROM-UNESCO, Roma, 1999.
- [39] Chen, X., Wu S., Zhou J., *Construction and Building Materials*, **40**, 869, 2013.
- [40] Al-Omari, A., Beck K., Brunetaud X., et al., *Engineering Geology*, **185**, 71, 2015.
- [41] Rodriguez-Navarro, C., Doehne E., *Earth Surface Processes and Landforms: The Journal of the British Geomorphological Research Group*, **24**(3),191, 1999.
- [42] Siegesmund, S., Snethlage R., *Stone in architecture: properties, durability*, Springer, Berlin, Heidelberg, 2011
- [43] Palchik, V., Hatzor Y., *Rock Mechanics and Rock Engineering*, **37**(4),331, 2004.
- [44] Ruedrich, J., Kirchner D., Siegesmund S., *Environmental Earth Sciences*, **63**(7-8),1573, 2011.
- [45] Benavente, D., Martínez-Verdú F., Bernabeu A., et al., *Color Research & Application: Endorsed by Inter-Society Color Council*, **28**(5), 343, 2003.
- [46] Rodrigues, J.D., Grossi A., *Journal of Cultural Heritage*, **8**(1), 32, 2007.
- [47] Grossi, C.M., Brimblecombe P., Esbert R.M., et al., *Color Research & Application: Endorsed by Inter-Society Color Council*, **32**(4), 320, 2007.